ISSN 0023-1584, Kinetics and Catalysis, 2006, Vol. 47, No. 4, pp. 501–510. © MAIK "Nauka/Interperiodica" (Russia), 2006.
Original Russian Text © E.Z. Utyanskaya, B.V. Lidskii, S.V. Goryachev, A.E. Shilov, 2006, published in Kinetika i Kataliz, 2006, Vol. 47, No. 4, pp. 518–527.

Kinetics and Mechanism of Adenosine 5'-Triphosphate Hydrolysis Catalyzed by the Cu^{2+} Ion: The Role of Conformation and the Catalytic Effect of the OH^- Ion

E. Z. Utyanskaya[a], B. V. Lidskii[b], S. V. Goryachev[a], and A. E. Shilov[a]

[a] *Emanuel Institute of Biochemical Physics, Russian Academy of Sciences, Moscow, 117977 Russia*
[b] *Semenov Institute of Chemical Physics, Russian Academy of Sciences, Moscow, 117977 Russia*
e-mail: neuhaus@center.chph.ras.ru

Received June 17, 2004

Abstract—The kinetics of 5'-ATP hydrolysis catalyzed by the Cu^{2+} ion has been investigated by HPLC in the pH range 5.6–7.8 at 25°C. Two series of experiments differing in the initial $[Cu \cdot ATP]_0$ (1 : 1) concentration have been carried out. The reaction was being conducted up to ≈40% ATP conversion. The $(CuATP^{2-})_2OH^-\{DOH^-\}$ complex, which consists of two monomeric $Cy(CuATP^{2-})$ molecules (in which the N7 atom and the γ-phosphate group are coordinated to Cu^{2+}), is responsible for the formation of $CuADP^- + P_i$ (P_i is an inorganic phosphate). The highest possible DOH^- concentration at a given pH is reached at the initial stage of hydrolysis. The pH value at which the highest initial rate of ADP formation is reached (pH_{max} ($w_{0,\,ADP}$)) decreases as the D concentration increases. At $pH > pH_{max}$, the decrease in the ADP formation rate in the course of the processes is pH-independent and, once an ATP conversion of 20–26% is reached, hydrolysis proceeds in a steady-state regime such that ADP and AMP form from ATP by parallel reactions. The participation of the OH^- ion in the catalysis of the formation of hydrolysis intermediates is considered.

DOI: 10.1134/S0023158406040057

The problem of determining the chemical mechanism of the conversion of the ATP hydrolysis energy into other kinds of energy is the central problem of bioenergetics. Therefore, information on the detailed mechanism of this process and on the principles of catalysis in simple model systems is of great interest [1, 2]. ATPase systems, which catalyze both ATP hydrolysis to ADP + P_i (P_i is an inorganic phosphate) and ATP synthesis, are metalloenzymes containing one or more metal ions at their active site [2–7]. The hydrolysis of ATP and other polyphosphates catalyzed by many protein enzymes shows complicated kinetics, and, in many cases, the conformational change of the enzyme is the rate-determining step [6–11]. Experimental studies have demonstrated that ATPases contain catalytic functional groups that perform a rapid and, according to some authors [8–10], reversible hydrolysis of ATP to enzyme-bound ADP + P_i. Furthermore, ATPases have groups participating in the deactivation of hydrolysis intermediates. As a consequence, the enzyme changes its conformation to desorb the products.

Recent studies in the design of model systems involving metal ions have shown that these catalytic systems have a complex composition and that the formation of hydrolysis products is characterized by complicated kinetics [12–31]. The following points are still unclear: the way P–O–P bonds in 5'-ATP–metal ion complexes break, the composition of active complexes and hydrolysis products, and the order of hydrolysis steps.

Numerous kinetic studies have dealt with the analysis of the initial dephosphorylation rates of 5'-ATP and its complexes with M^{2+} ions. However, the key to understanding the role of 5'-ATP in the conformational changes of enzymes is in the conversion of 5'-ATP–metal ion hydrolysis intermediates and in the effects of ligands on this conversion.

In our earlier studies, we suggested a structural model for the hydrolysis site. In this model, the active ion, $M^{2+}OH^-$, occupies a place opposite the breaking P_γ–OP_β bond owing to the coordination of M^{2+} to the N7 atom of the adenine base and to the O^- atom of the γ-phosphate group of the ATP molecule undergoing hydrolysis, yielding the cyclic (Cy) conformation of the $MATP^{2-} \cdot OH_2$ complex (see Fig. 1a in [32, 33]). Based on structural and kinetic data, we assumed that, in the cyclic monomeric conformation of $ZnATP^{2-}$, the Zn^{2+} ion interacts directly with one O^- atom of the γ-phosphate group and indirectly, through the coordinated

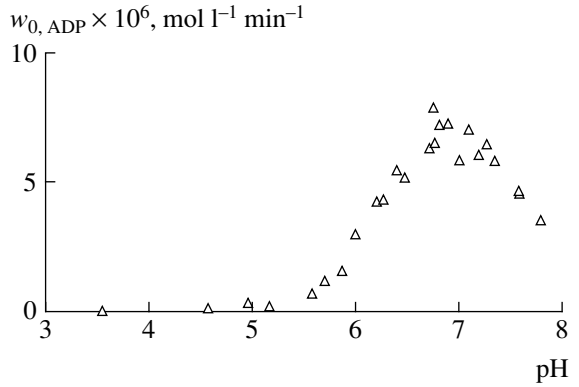

Fig. 1. Initial ADP formation rate ($w_{0,\ ADP}$) as a function of pH at 25°C for series I runs. The initial Cu · ATP (1 : 1) concentration is $[Cu \cdot ATP]_0 = (2.07 \pm 0.03) \times 10^{-3}$ mol/l.

H_2O molecule, with another O^- atom. The $Zn^{2+}OH^-$ ion resulting from the detachment of a proton from the coordinated water molecule is located opposite the γ-P atom [34–37]. Later, we obtained kinetic and thermodynamic data confirming this structure of the active monomeric cycle [35–37]. We found that the $Zn^{2+}OH^-$ ion is active in the hydrolysis of ATP to ADP + P_i only when the phosphate chain in the cyclic conformation both in the dimer $(ZnATP^{2-})_2H^+OH^-$ and in the monomer $ZnATP^{2-}OH^-$ [32, 33, 35–37]. At the active site of the dimer, the N1 atom of the adenine base of another $ZnATP^{2-}$ molecule detaches a proton from the coordinated H_2O molecule that is opposite the γ-phosphate group. This is followed by a fast reversible step in which the proton is transferred so as to form a hydrogen bond between the γ-phosphate group bonded to Zn^{2+} and the N1 atom of the second $ZnATP^{2-}$ molecule (which is in the conformation A). The hydrolysis of the dimeric and trimeric association species determines the kinetics of the pH-independent channel, and the hydrolysis of the $CyOH^-$ monomer determines the kinetics of the pH-dependent channel [32, 33, 35–38]. The rate and equilibrium constants of proton transfer reactions involving the common basic catalyst are much higher for the $ZnATP^{2-}$ trimers than for the $ZnATP^{2-}$ dimers [33, 38]. The open (Op) $ZnATP^{2-}$ conformers, in which Zn^{2+} is bonded only to the phosphate chain, are assumed to be β,γ-conformers (Op and $OpOH^-$ species; see Fig. 1b in [32]). They are inactive in hydrolysis and transform into active γ-complexes via a series of isomerization steps [32]. The formation of $Cy(ZnATP^{2-})$ from $Op(ZnATP^{2-})$ occurs slowly at pH >8.5 and is catalyzed by the H_3O^+ ion [32]. In both of the pH-independent and pH-dependent channels of $ZnATP^{2-}$ hydrolysis, the attacking nucleophile is the coordinated OH^- ion located opposite the γ-phosphate group.

The initial rate of the pH-dependent hydrolysis of the Cu · ATP (1 : 1) complex at 50 and 25°C was measured by chemical analysis for inorganic phosphate in earlier studies. It was demonstrated that, at 50°C and concentrations of 10^{-4} to 10^{-2} mol/l, the reaction is formally second-order with respect to the Cu · ATP complex and the initial hydrolysis rate as a function of pH passes through a maximum, whose position is temperature-dependent [1, 2, 16]. It was assumed that, in the ascending and descending branches of the initial rate-vs.-pH curve, the species active in ADP formation are $[Cu_3(ATP)_2(OH)]^{3-}$ and $(CuATP^{2-})_2(OH^-)$, respectively.

We assume that common features of the hydrolyses of the $(ZnATP^{2-})_2H^+OH^-$ and $(CuATP^{2-})_2$ complexes are that the intermediates are dimers and have the same geometry [34]. The equilibrium constant for the deprotonation of the coordinated H_2O molecule in the Cy-form of $ZnATP^{2-}$ is 0.84×10^{-9} mol/l [32, 36], and the formal equilibrium constant for the deprotonation of the coordinated H_2O molecule in $CuATP^{2-} \cdot OH_2$ is 6.75×10^{-9} mol/l [16]. Therefore, as distinct from the Zn^{2+}-containing dimer, the $(CuATP^{2-} \cdot OH_2)_2$ dimer readily loses a proton.

Here, we report a quantitative study of the formal hydrolysis kinetics of the $(CuATP^{2-} \cdot OH_2)_2$ complex at 25°C. In this study, which included two series of experiments differing in terms of the initial Cu–ATP concentration, we not only measured the initial rates of ADP formation and ATP consumption but also recorded kinetic curves up to ≈40% ATP conversion in the pH range 3.5–7.8. The ultimate goal of this study was to establish the order in which conformationally different intermediates are formed and converted in the hydrolysis of ATP to the final products (ADP and AMP), to elucidate the role of the H_3O^+ and OH^- ions in the sequence of hydrolysis steps, and to understand why the initial rate as a function of pH passes through a maximum.

Our study consists of two parts. The first is devoted to the formal kinetics of hydrolysis. In the second, we establish the order of hydrolysis steps and determine, by numerical simulation, the rate and equilibrium constants for the steps of the conversion of hydrolysis intermediates.

EXPERIMENTAL

ATP was purchased either from Reanal (Hungary) or from Fluka (adenosine 5'-triphosphate disodium salt hydrate, Biochemika, 97% according to HPLC). Commercial ATP was reprecipitated from its aqueous solution with ethanol and was vacuum-dried to a constant weight at ≈20°C. ATP solutions were prepared immediately before measurements using thrice distilled water. The initial nucleoside 5'-triphosphate concentration in the solutions was determined spectrophotometrically (λ = 259 and 260 nm, ε_M = 15000 l mol^{-1} cm^{-1}).

$Cu(NO_3)_2 \cdot 3H_2O$ (Fluka, >99%) was stored over calcined $CaCl_2$ in a desiccator. $Cu(NO_3)_2$ solutions with a preset salt concentration were prepared under flowing argon and were stored in an $HClO_4$ solution with pH ≈ 4.1. The concentration of Cu^{2+} was determined spectrophotometrically from absorbance data for sodium ethylenediaminetetraacetate in the region of the existence of the Cu^{2+} complex (pH 5–9) [40]; $\varepsilon_M = 98.8$ l mol^{-1} cm^{-1}; $\lambda = 725$, 730, and 735 nm). Parallel measurements were performed in an acetate buffer (pH 5.8–8.5) and at λ = 800 nm ($\varepsilon_M = 12.3$ l mol^{-1} cm^{-1}) [40]. The results were averaged, and the discrepancy between data obtained under different conditions appeared to be 1–2%. Electronic spectra were recorded on an SF-26 spectrophotometer. pH was measured in a microcell with an I-135-M1 instrument in kinetic experiments and with an EV-74 instrument in chemical analysis (sample size ≈0.5 cm^3). The instruments were calibrated against standard buffer solutions at 25°C. Kinetic runs were carried out at 25°C in a thermostated glass cell under flowing argon using an earlier described procedure [35–37, 39]. The reaction was initiated by adding, to an ATP solution containing $NaClO_4$, an appropriate amount of a $Cu(NO_3)_2$ solution with a known salt concentration and an NaOH solution to raise pH to the preset value. Before the reaction and at certain intervals during the reaction, the reaction mixture was sampled with a graduated pipette. The samples were dissolved in an appropriate volume of an $HClO_4$ solution and were diluted so that pH was ≈3 and the total concentration of nucleoside 5'-phosphates was ≈(3–4) × 10^{-4} mol/l. Next, the samples were quickly frozen and were stored at –18 to –20°C. For analysis, a sample was thawed and centrifuged and a 20-μl aliquot was injected into the sampler of a chromatograph. Individual 5'-nucleotides in the 5'-ATP hydrolysis products were quantified by reversed-phase ion-pair high-performance liquid chromatography (HPLC) using standard glass columns packed with Separon SGX-18 (Czech Republic). The chromatographic determination of 5'-adeninenucleotides is detailed elsewhere [39]. The ion-pair agent was tetrabutylammonium hydrogen sulfate. In order to study ATP hydrolysis catalyzed by the Cu^{2+} ion, which absorbs UV light, we modified the earlier reported procedure by introducing ≈10^{-3} mol/l of the complexon pyrophosphate (PP) into the mobile phase. In the absence of PP, we observed a broad asymmetric peak at the beginning of the chromatogram ($\tau \approx 5$ min). The tail of this peak extended up to the AMP peak. We consider this peak to be due to the sorption of Cu^{2+} ions on residual surface silanol groups. Adding PP to the eluent brings about a narrow peak due to the complex $Cu^{2+} \cdot PP \cdot TBA^+$ at the beginning of the chromatogram (τ = 3.2 min; capacity coefficient, $k' = 0.26$). With a standard mobile phase containing 0.12 mol/l of KH_2PO_4, (2.9–3.0) × 10^{-3} mol/l of TBA^+, and 7–8 vol % CH_3OH, the free nucleoside 5'-phosphates not coordinated to Cu^{2+} are chromatographed with $\tau_{AMP} \approx 11$ min (k' = 1.9), $\tau_{ADP} \approx 13.7$ min ($k' = 2.6$), and $\tau_{ATP} \approx 16.5$ min ($k' = 3.3$). The PP concentration in the eluent is three orders of magnitude higher than the ATP concentration in the retained volume (10^{-6} mol/l). The initial ATP consumption rate (w_0) was derived from the initial portion of the ATP concentration curve:

$$w_{0,\,ATP} = (-d\alpha_{ATP}/dt)[NuP]_0, \quad (1)$$

where $[NuP]_0 = ([ATP] + [ADP] + [AMP])_0$, NuP is nucleoside 5'-phosphate, and α_{ATP} is the ATP mole fraction. The initial ADP formation rate was derived from the initial portion of the ADP buildup curve:

$$w_{0,\,ADP} = (d\alpha_{ADP}/dt)[NuP]_0, \quad (2)$$

where α_{ADP} is the ADP mole fraction. The reaction rate at the steady-state ADP and AMP formation stage was determined in a similar way. Two or three replica measurements were done for each sample, and the results differing by no more than 0.1–0.2 mol % were averaged.

RESULTS AND DISCUSSION

Table 1 lists measurement conditions for the runs that were included in the analysis. Two series of kinetic experiments were carried out, which differed in terms of the initial $Cu \cdot ATP$ concentration: in series I, $[Cu \cdot ATP]_0 = (2.07 \pm 0.03) \times 10^{-3}$ mol/l and pH 3.6–7.8 (runs 1–25); in series II, $[Cu \cdot ATP]_0 = (2.92 \pm 0.03) \times 10^{-3}$ mol/l and pH 5.7–7.8 (runs 26–33). In the pH range examined (5.6–7.8), $CuATP^{2-}$ is the most abundant complex species. The $CuATP^{2-}$ concentration in either series of runs is nearly constant at pH 5.6–7.3 and decreases slightly at pH 7.3–7.8 (Table 1). In series I, $w_{0,\,ADP}$ as a function of pH passes through a maximum at pH 6.76 (Fig. 1). In series II, this maximum occurs at pH 6.47 (Fig. 2). In an earlier series of experiments carried out at $[Cu \cdot ATP]_0 = 1 \times 10^{-3}$ mol/l and 25°C, this peak was observed at pH 7.26 [16] (in that study, the initial P_i formation rate was measured under the assumption that the only hydrolysis product is ADP). The ADP and AMP formation and ATP consumption curves for the ascending branch of the $w_{0,\,ADP}$-vs.-pH curve are very different from the same curves for the descending branch. In Fig. 3, we plot the ATP consumption and ADP and AMP formation curves for the hydrolysis of the $Cu \cdot ATP$ (1 : 1) complex in a comparatively acidic region (pH (*1*) 5.58, (*2*) 6.00, and (*3*) 6.27) for the ascending branch of the $w_{0,\,ADP}$-vs.-pH curve (series I runs). The reactions were usually run up to 33–40% ATP conversion. Because hydrolysis at pH < 5.7 was very slow, it was conducted only to 15–18% ATP conversion. In Table 1, we specify the ATP conversion values (%) up to which the initial portion of the ADP formation curve is linear. In this linear

Table 1. Experimental conditions for pH 3.5–7.8

Series no.	Run no.	pH*	$[NuP]_0 \times 10^3$, mol/l	$[Cu^{2+}]_0 \times 10^3$, mol/l	$[NaClO_4]$, mol/l	$[Cu \cdot ATP]_0 \times 10^3$, mol/l	$[CuATP^{2-}]_0 \times 10^3$, mol/l	$w_{0,\,ADP} \times 10^6$, mol l^{-1} min^{-1}	$w_{0,\,ATP} \times 10^6$, mol l^{-1} min^{-1}	Conversion in terms of [Cu · ATP]**, mol %	Change in [AMP]***, mol %
I	1	3.55 ± 0.02	2.22	2.16	0.126	2.12	0.573	0.022 ± 0.006	0.018 ± 0.012	0.3	No change
	2	4.58 ± 0.01	2.19	2.12	0.124	2.08	1.60	0.137 ± 0.008	0.138 ± 0.013	2.0	″
	3	4.96 ± 0.01	2.18	2.12	0.112	2.07	1.82	0.318 ± 0.011	0.327 ± 0.013	3.5	″
	4	5.17 ± 0.01	2.15	2.09	0.110	2.06	1.84	0.198 ± 0.006	0.205 ± 0.009	3.4	″
	5	5.58 ± 0.05	2.17	2.11	0.111	2.10	1.96	0.670 ± 0.016	0.714 ± 0.019	8.9	″
	6	5.70 ± 0.03	2.17	2.11	0.110	2.09	1.97	1.16 ± 0.03	1.22 ± 0.04	12.8	″
	7	5.87 ± 0.02	2.17	2.11	0.110	2.09	1.99	1.52 ± 0.06	1.51 ± 0.14	18.5	″
	8	6.00 ± 0.02	2.18	2.11	0.109	2.03	1.93	2.92 ± 0.05	3.02 ± 0.08	12.3	″
	9	6.20 ± 0.04	2.16	2.11	0.108	2.08	1.98	4.24 ± 0.13	4.40 ± 0.12	10.5	Increases by 0.4
	10	6.27 ± 0.03	2.17	2.10	0.109	2.04	1.94	4.31 ± 0.05	4.64 ± 0.18	10.0	Increases by 0.7
	11	6.40 ± 0.02	2.16	2.10	0.105	2.08	1.97	5.43 ± 0.21	5.21 ± 0.27	6.6	Increases by 0.1
	12	6.48 ± 0.02	2.16	2.10	0.108	2.08	1.97	5.17 ± 0.19	5.59 ± 0.18	10.0	Increases by 0.5
	13	6.71 ± 0.01	2.16	2.10	0.105	2.08	1.95	6.33 ± 0.40	6.75 ± 0.46	3.6	Increases by 1.0
	14	6.76 ± 0.03	2.17	2.10	0.117	2.09	1.96	7.90 ± 1.09	8.43 ± 1.13	9.0	Increases by 0.4
	15	6.77 ± 0.03	2.20	2.12	0.119	2.10	1.95	6.53 ± 1.02	7.13 ± 1.07	9.0	Increases by 0.5
	16	6.81 ± 0.03	2.16	2.10	0.111	2.09	1.96	7.23 ± 1.54	7.70 ± 1.61	4.4	Increases by 0.2
	17	6.90 ± 0.02	2.16	2.10	0.112	2.09	1.93	7.29 ± 0.99	7.43 ± 1.17	5.1	Increases by 0.1
	18	7.00 ± 0.03	2.15	2.10	0.110	2.08	1.91	5.85 ± 0.11	6.10 ± 0.12	6.3	Increases by 0.2
	19	7.09 ± 0.03	2.16	2.10	0.105	2.09	1.90	7.06 ± 0.34	7.42 ± 0.41	6.0	Increases by 0.3
	20	7.20 ± 0.02	2.15	2.09	0.111	1.96	1.75	6.07 ± 0.28	6.53 ± 0.30	4.7	Increases by 0.5
	21	7.27 ± 0.04	2.14	2.10	0.107	2.08	1.81	6.48 ± 0.18	7.01 ± 0.22	6.2	Increases by 0.5
	22	7.35 ± 0.02	2.15	2.09	0.109	2.08	1.77	5.86 ± 0.32	6.17 ± 0.30	5.8	Increases by 0.3
	23	7.58 ± 0.03	2.14	2.08	0.108	2.07	1.61	4.66 ± 0.26	4.78 ± 0.38	5.7	Increases by 0.4
	24	7.59 ± 0.02	2.15	2.08	0.109	2.04	1.59	4.56 ± 0.17	4.94 ± 0.24	6.4	Increases by 0.3
	25	7.79 ± 0.02	2.14	2.08	0.106	2.06	1.45	3.53 ± 0.15	3.95 ± 0.16	4.8	Increases by 0.4
II	26	5.69 ± 0.03	3.13	3.05	0.101	2.99	2.81	3.14 ± 0.06	3.33 ± 0.07	19.0	Increases by 1.2
	27	5.87 ± 0.02	3.09	3.02	0.098	2.96	2.82	3.41 ± 0.04	3.61 ± 0.04	20.0	Increases by 1.2
	28	6.08 ± 0.02	3.08	3.01	0.113	2.90	2.76	6.55 ± 0.17	6.92 ± 0.15	12.0	Increases by 0.5
	29	6.36 ± 0.03	3.08	3.02	0.105	2.93_5	2.78	7.85 ± 0.47	8.06 ± 0.57	5.6	Increases by 0.3
	30	6.47 ± 0.04	3.09	3.02	0.110	2.90	2.74	10.3 ± 0.9	11.8 ± 1.1	5.2	Increases by 0.2
	31	6.86 ± 0.03	3.06	3.00	0.101	2.89	2.68	7.98 ± 0.25	7.97 ± 0.25	6.6	Increases by 0.1
	32	7.57 ± 0.03	3.06	2.98	0.101	2.91	2.27	7.01 ± 0.20	7.11 ± 0.22	6.7	Increases by 0.1
	33	7.79 ± 0.04	3.06	2.98	0.095	2.93	2.06	6.38 ± 0.44	6.54 ± 0.45	6.7	Increases by 0.1

Note: $[NuP]_0$ is the total initial concentration of nucleoside 5'-phosphates; $[NaClO_4]$ is the $NaClO_4$ concentration in the cell; [Cu · ATP] means equivalent amounts of Cu^{2+} and ATP present in the solution, without taking into account the real speciation; $[Cu \cdot ATP]_0$ is calculated from the initial mole fraction α_{0ATP}, which is derived either by extrapolating the initial linear portion of the ATP consumption curve to $t \longrightarrow 0$ or by analyzing the nucleotide composition of the solution before pH stabilization; $[CuATP^{2-}]_0 = a[Cu \cdot ATP]_0$, where a is the mole fraction of $CuATP^{2-}$ in the totality of species at a given pH and 25°C according to [16]; $w_{0,\,ADP}$ is the initial ADP formation rate derived from the initial linear portion of the ADP buildup curve; $w_{0,\,ATP}$ is the initial ATP consumption rate derived from the ATP consumption curve. The error ranges placed at the initial rate values are for 95% confidence probability.

* Mean pH value in the run and pH control accuracy.

** Cu · ATP conversion up to which the initial portions of the ATP consumption and ADP formation curves are linear.

*** Change in the AMP concentration for the initial linear portions of the ATP consumption and ADP formation curves.

region, there is an induction period in AMP formation. The amounts of AMP forming in this region are also indicated in Table 1. The ATP consumption and ADP formation rates are nearly equal in the linear region, while the formation rate of the intermediate yielding AMP can be neglected there. It follows from Fig. 3 that, as pH is increased from 6.00 to 6.27, the ATP conversion value limiting the initial ADP formation and ATP consumption linearities decreases and the reaction rate falls progressively more sharply. In run 5 (pH 5.58), nearly all of the kinetic measurements refer to the initial linear region; however, only the data plotted in Fig. 3 were used in calculating the initial reaction rates. As pH grows in the ascending branch of the $w_{0,\,ADP}$-vs.-pH curve, the final portions of the ADP and AMP formation and ATP consumption curves change. As the ADP formation rate maximum is approached in series I runs (at pH ≥ 6.40), the ADP and AMP concentrations increase and the ATP concentration decreases with time at a nearly constant rate in the final period of time. The total ADP and AMP formation rate is equal to the ATP consumption rate once ≈26% ATP conversion is reached, indicating that ADP and AMP form by parallel reactions from ATP. For series I runs at pH ≥ 6.4, we indicate, in Table 2, the ATP conversion values at which steady-state hydrolysis and the parallel formation of ADP and AMP begin. Also listed are the almost constant values of the ATP consumption and ADP and AMP formation rates (w_{const}) and $w_{const,\,AMP}/w_{const,\,ATP}$, $w_{0,\,ADP}/w_{const,\,ADP}$, and $w_{0,\,ATP}/w_{const,\,ATP}$ ratios. Figure 4 shows the ATP consumption and ADP and AMP formation curves for run 19 (series I, pH 7.09). These curves are typical for the descending branch of the pH dependence of the initial rate. The initial portions of the ATP consumption and ADP formation curves are linear. Another linearity is observed starting at ≈26% ATP conversion, with $w_{const,\,ADP} + w_{const,\,AMP} = w_{const,\,ATP}$. At $pH \geq pH_{max}$ in experimental series I, the $w_{0,\,ADP}/w_{const,\,ADP}$ and $w_{const,\,AMP}/w_{const,\,ATP}$ ratios are almost invariable considering the scatter of data and are 4.59 ± 0.68 and $0.14_5 \pm 0.03$, respectively, for 11 runs.

Similar regularities are observed in experimental series II. Figure 5 plots the ATP consumption and ADP and AMP formation curves for the ascending branch of the initial rate-vs.-pH curve (run 27 in Table 1). Figure 6 shows the same curves for the descending branch (run 32 in Table 1). In Table 2, the descending branch of the initial rate-vs.-pH curve is represented by runs 31–33 of series II. The $w_{0,\,ADP}/w_{const,\,ADP}$ ratio in runs 31 and 32 (4.52 ± 0.23) is equal to that in series I within the measurement error. The $w_{const,\,AMP}/w_{const,\,ATP}$ ratio in series II ($0.11_5 \pm 0.01$) is close to the same ratio in series I.

As in the case of the hydrolysis of the $ZnATP^{2-}$ complex, we assume that only the cyclic form of $CuATP^{2-}$, in which the Cu^{2+} ion is bonded to the N7 atom of its own adenine base and to its own γ-phosphate group, is active in the ADP + P_i formation reaction. The data

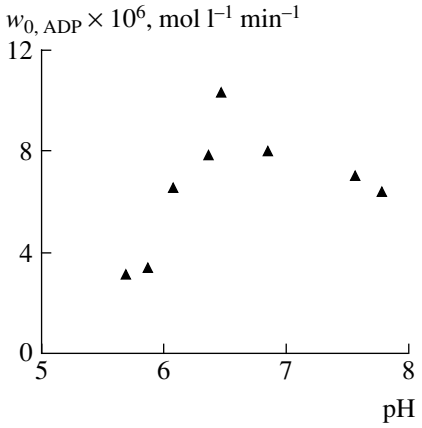

Fig. 2. Initial ADP formation rate ($w_{0,\,ADP}$) as a function of pH at 25°C for series II runs. The initial Cu · ATP (1 : 1) concentration is $[Cu \cdot ATP]_0 = (2.92 \pm 0.03) \times 10^{-3}$ mol/l.

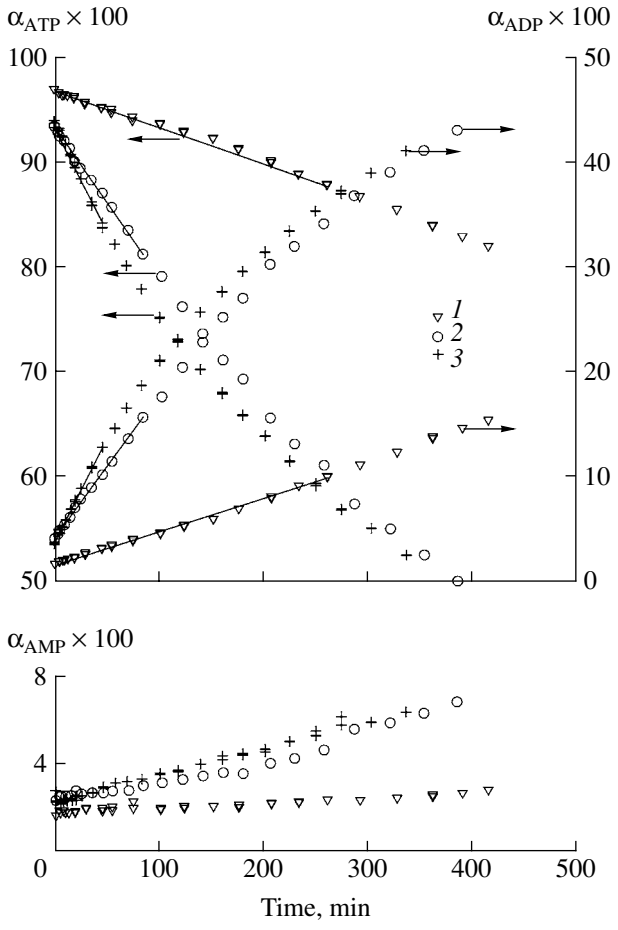

Fig. 3. ATP consumption and ADP and AMP formation kinetics in the hydrolysis of the Cu · ATP (1 : 1) complex: (*1*) pH 5.58 ($[Cu \cdot ATP]_0 = 2.10 \times 10^{-3}$ mol/l), (*2*) pH 6.00 ($[Cu \cdot ATP]_0 = 2.03 \times 10^{-3}$ mol/l), and (*3*) pH 6.27 ($[Cu \cdot ATP]_0 = 2.04 \times 10^{-3}$ mol/l). The solid lines indicate the linear portions of the curves from which the initial rates were derived.

Table 2. Nearly constant ATP disappearance and ADP and AMP appearance rates, and the ATP conversions starting at which these rates are constant

Series no.	Run no.	pH	$w_{const, ATP} \times 10^6$, mol l^{-1} min^{-1}	$w_{const, ADP} \times 10^6$, mol l^{-1} min^{-1}	$w_{const, AMP} \times 10^6$, mol l^{-1} min^{-1}	$w_{const, AMP}/w_{const, ATP}$	$w_{0, ADP}/w_{const, ADP}$	$w_{0, ATP}/w_{const, ATP}$	ATP conversion, %
I	11	6.40	2.15 ± 0.11	1.87 ± 0.22	0.28 ± 0.02	0.13_2	2.9_1	2.4_2	$26._5$
	12	6.48	2.07 ± 0.12	1.76 ± 0.07	0.31 ± 0.07	0.15_2	2.9_4	2.7	$26._5$
	13	6.71	2.49 ± 0.18	2.08 ± 0.14	0.41 ± 0.07	0.16_6	3.0_5	2.7_1	$26._5$
	14	6.76	1.92 ± 0.10	1.70 ± 0.08	0.22 ± 0.01	0.11_6	4.6_6	4.4_0	$22._2$
	15	6.77	2.19 ± 0.27	1.99 ± 0.21	0.23 ± 0.07	0.10_5	3.2_8	3.2_6	$25._1$
	16	6.81	2.27 ± 0.11	1.90 ± 0.10	0.38 ± 0.02	0.16_6	3.8_1	3.3_9	$26._7$
	17	6.90	2.16 ± 0.07	1.79 ± 0.06	0.37 ± 0.02	0.16_9	4.0_7	3.4_5	$28._1$
	18	7.00	1.49 ± 0.13	1.33 ± 0.11	0.16 ± 0.04	0.11	4.4_2	4.1_0	$25._6$
	19	7.09	1.68 ± 0.18	1.39 ± 0.15	0.28 ± 0.06	0.16_7	5.0_6	4.4_1	$27._0$
	20	7.20	1.25 ± 0.35	1.06 ± 0.28	0.17 ± 0.08	0.13_4	5.7_3	5.2_1	$18._0$
	21	7.27	1.52 ± 0.10	1.30 ± 0.09	0.22 ± 0.02	0.14_6	4.9_8	4.6_0	$26._6$
	22	7.35	1.34 ± 0.16	1.15 ± 0.15	0.19 ± 0.02	0.14_3	5.1_2	4.6_2	$26._6$
	23	7.58	1.29 ± 0.21	1.03 ± 0.19	0.23 ± 0.03	0.17_6	4.5_1	3.7_0	$22._0$
	24	7.59	1.72 ± 0.08	1.47 ± 0.06	0.28 ± 0.04	0.16_4	–	–	$21._0$
	25	7.79	0.86 ± 0.05	0.73 ± 0.06	0.14 ± 0.02	0.16_2	4.8_7	4.5_8	$18._0$
II	31	6.86	2.70 ± 0.16	2.40 ± 0.15	0.28 ± 0.02	0.10_3	–	–	$24._0$
	32	7.57	1.81 ± 0.07	1.61 ± 0.05	0.20 ± 0.04	0.11	4.3_6	3.9_4	$22._7$
	33	7.79	1.55 ± 0.06	1.36 ± 0.06	0.18 ± 0.04	0.12	4.6_8	4.2_2	$18._2$

reported for the monomeric complex $ZnATP^{2-}$ [36] suggest that, at pH < 8.0 in our experiments, the monomers Op($CuATP^{2-}$) and Cy($CuATP^{2-}$) rapidly reach equilibrium. Either species is characterized by a deprotonation equilibrium constant for the water molecule coordinated to Cu^{2+}:

$$\begin{aligned} &Cy \overset{+H_2O}{\rightleftharpoons} H_3O^+ + CyOH^-, \\ &K_{a, Cy} = [H_3O^+][CyOH^-]/[Cy], \end{aligned} \quad (3)$$

$$\begin{aligned} &Op \overset{+H_2O}{\rightleftharpoons} H_3O^+ + OpOH^-, \\ &K_{a, Op} = [H_3O^+][OpOH^-]/[Op]. \end{aligned} \quad (4)$$

The fractions of Cy($CuATP^{2-}$) and Op($CuATP^{2-}$) in the monomer are, respectively, 0.67 and 0.33 [19]; $pK_{a, obs} = 8.17 \pm 0.02$ for $CuATP^{2-}$ at 25°C [16].

In the calculation of the initial [$OpOH^-$] and [$CyOH^-$] values (for example, for run 12, series I, pH 6.48), we used the following data: the total concentration of nucleoside 5'-phosphates in the reaction mixture before the reaction, determined spectrophotometrically, is $[NuP]_0 = 2.16 \times 10^{-3}$ mol/l; $[Cu \cdot ATP]_0 = 2.08 \times 10^{-3}$ mol/l, as calculated from the initial ATP mole fraction determined by chromatographing the initial reaction mixture ($ATP_0 = 0.965$); and $[CuATP^{2-}]_0 = a \times 2.08 \times 10^{-3}$ mol/l, where $a = 0.946$ (see Fig. 4 and Table 5 in [16]). At pH 6.48, the Cu · ATP (1 : 1) complex yields a rapidly equilibrating mixture of $CuATP^{2-}$ (mole fraction 0.946), $CuATP^{2-}OH^-$ (mole fraction 0.025), and $HATP^{3-}$ (the balance) [16]. The balance equation for $[CuATP^{2-}]$ at the initial time point is

$$[CuATP^{2-}]_0 = [Cy]_0 + [Op]_0 + 2[D]_0, \quad (5)$$

where $[Cy]_0$ and $[Op]_0$ are the concentrations of the cyclic and open monomeric forms of $CuATP^{2-}$, and $[D]_0$ is the concentration of the dimeric form of $CuATP^{2-}$ consisting of two monomeric Cy molecules.

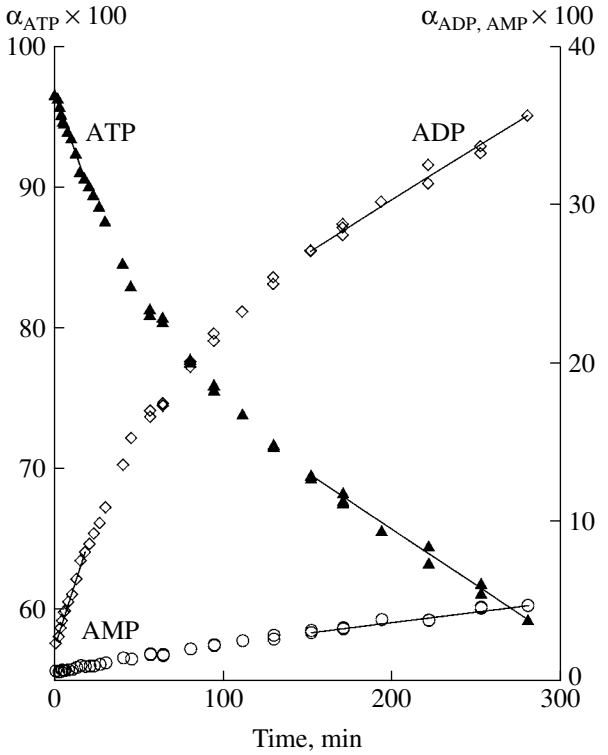

Fig. 4. ATP consumption and ADP and AMP formation kinetics in the hydrolysis of the Cu · ATP (1 : 1) complex at pH 7.09 and $[Cu \cdot ATP]_0 = 2.09 \times 10^{-3}$ mol/l.

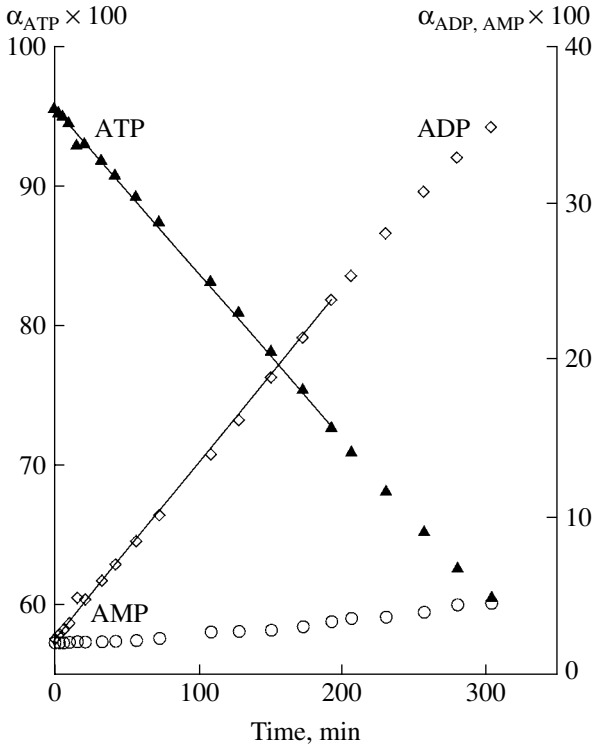

Fig. 5. ATP consumption and ADP and AMP formation kinetics in the hydrolysis of the Cu · ATP (1 : 1) complex at pH 5.87 and $[Cu \cdot ATP]_0 = 2.96 \times 10^{-3}$ mol/l.

This equation implies that the dimer is rapidly equilibrated with the monomers. At $t = 0$, $[D]_0 = 2.13_4 \times 10^{-4}$ mol/l, $[Cy]_0 = 1.03 \times 10^{-3}$ mol/l, and $[Op]_0 = 0.51 \times 10^{-3}$ mol/l. The deprotonated species concentrations $[CyOH^-]_0$ and $[OpOH^-]_0$ were calculated using Eqs. (3) and (4) with preset values of $K_{a, Cy}$ and $K_{a, Op}$. Initially, it was assumed that $K_{a, Op}/K_{a, Cy} = 1.95$, as in the case of $ZnATP^{2-}$ [32, 36, 37]. This assumption means that the structural difference between the Cy and Op monomers of $MATP^{2-}$, which is manifested as a difference between $K_{a, Cy}$ and $K_{a, Op}$, is approximately the same for $M^{2+} = Zn^{2+}$ and Cu^{2+}. The $K_{a, Cy}$ and $K_{a, Op}$ values calculated under this assumption are 5.15×10^{-9} and 1.00×10^{-8} mol/l, respectively. The $[CyOH^-] + [OpOH^-]$ value for these $K_{a, Cy}$ and $K_{a, Op}$ values, pH 6.70, and $[Cu \cdot ATP]_0 = 1 \times 10^{-3}$ mol/l is calculated to be 2.8×10^{-5} mol/l. Potentiometric data obtained under the same conditions lead to $[CuATP^{2-}OH^-] = 3.6 \times 10^{-5}$ mol/l, and the difference between the calculated and observed data for the overall balance of Cu · ATP species is 0.8%. At higher pH values of 6.9–7.8, as the proportion of the ions in the totality of species increases from 0.05 to 0.29, this difference increases to 1.1–2.5% at $[Cu \cdot ATP]_0 = 1 \times 10^{-3}$ mol/l and to 2.0–5.4% at $[Cu \cdot ATP]_0 = 2 \times 10^{-3}$ mol/l. In these calculations, the $Cy(CuATP^{2-})$ dimerization constant was taken to be 200 l/mol. A better agreement between the calculated $[CyOH^-] + [OpOH^-]$ value and potentiometric data is achieved with $K_{a, Cy} = 8.24 \times 10^{-9}$ mol/l and $K_{a, Op} = 1.00 \times 10^{-8}$ mol/l. For series I runs at $[Cu \cdot ATP]_0 = 2 \times 10^{-3}$ mol/l, the discrepancy between the calculated and observed data is 0.2% for pH 6.81 (run 16). For pH 6.9–7.8 (runs 17–25), the discrepancy as to the balance of Cu · ATP species is typically 0.1–0.8%. For pH 7.58 (run 23), this discrepancy is 1.3%. The maximum discrepancy, 2.7%, is observed for pH 7.58 (run 25). In series II, the difference between the calculated and observed $[CyOH^-] + [OpOH^-]$ values is 0.58% for pH 6.47 (run 30, $CuATP^{2-}OH^-$ ion fraction 2.4%) and 0.79% for pH 7.79 (run 33, $CuATP^{2-}OH^-$ ion fraction 0.29). These calculations demonstrate that the second variant of $K_{a, Cy}$ and $K_{a, Op}$ values provides a satisfactory fit to the observed pH dependence of $[CyOH^-] + [OpOH^-]$. Apparently, the structural difference between the $Cy(MATP^{2-})$ and $Op(MATP^{2-})$ species is not the same for Zn^{2+} and Cu^{2+}.

When calculating the fraction of the active species D, which consists of two $Cy(CuATP^{2-})$ monomers, we proceeded from the following considerations. We assumed that the dimerization constant of the $(ZnATP^{2+})_2H^+OH^-$ complex depends slightly on tem-

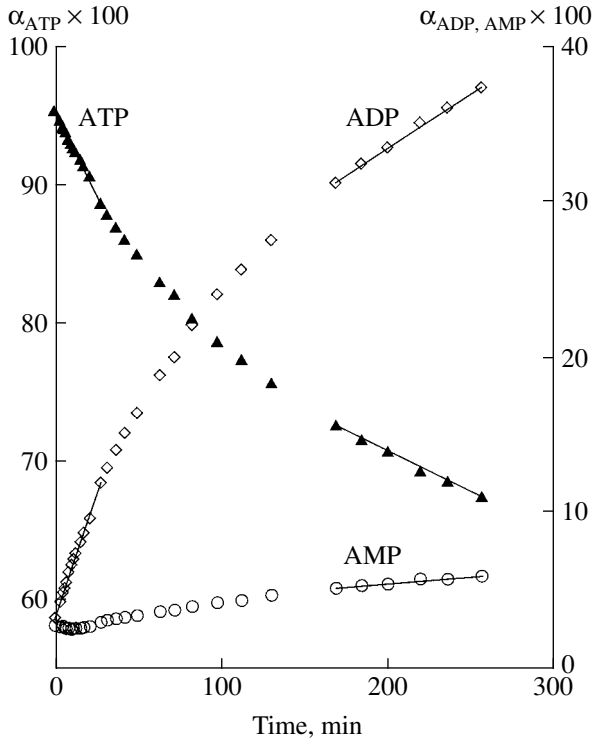

Fig. 6. ATP consumption and ADP and AMP formation kinetics in the hydrolysis of the Cu · ATP (1 : 1) complex at pH 7.57 and $[Cu \cdot ATP]_0 = 2.91 \times 10^{-3}$ mol/l.

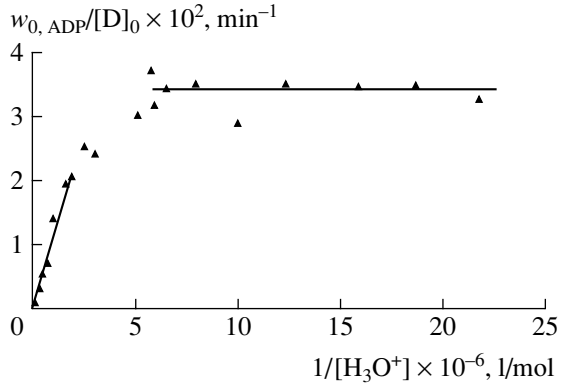

Fig. 7. Apparent ADP formation rate constant ($w_{0, ADP}/[D]_0$) versus $1/[H_3O^+]$ for the hydrolysis of the dimeric complex $(CuATP^{2-} \cdot OH_2)_2$ in series I runs at 25°C.

perature between 25 and 50°C. Earlier, we derived $K'_D = [D]_0/[Cy]_0^2 = 260$ l/mol from kinetic data for the hydrolysis of the dimeric Cy($ZnATP^{2-}$) complex at pH 7.1 and $T = 50$°C under the assumption that only the dimeric form of $ZnATP^{2-}$ undergoes hydrolysis. Accordingly, $K_D \approx 20$ l/mol for the unit monomer concentration [33]. A similar value of $K_D \approx 20$–30 l/mol was derived from the chemical shift of the H8 proton in the ^1H NMR spectrum as a function of the $ZnATP^{2-}$ concentration at 27°C and pD 7.2 [18]. The association constant of the $ZnATP^{2-}$ complex depends strongly on the $ZnATP^{2-}$ concentration. By considering the reactivity of the $ZnATP^{2-}$ dimers and trimers separately, we obtained $K'_D = 210$ l/mol for the dimeric Cy($ZnATP^{2-}$) complex (which determines the hydrolysis kinetics at comparatively low $ZnATP^{2-}$ concentrations of $<2.6 \times 10^{-3}$ mol/l) and a much higher value for the trimers [33].

The dimer $(ZnATP^{2+})_2 \cdot H^+OH^-$ forms through the stacking interaction between the adenine bases of two $ZnATP^{2-}$ molecules in the Cy($ZnATP^{2-}$) conformation and through the hydration of the terminal phosphate group by the water molecule that is coordinated to Zn^{2+} and belongs to the $ZnATP^{2-}$ molecule undergoing hydrolysis ($ZnATP^{2-}$ molecule in conformation B in Fig. 1c in [32]; see also scheme 2 in [34]). In the case of Zn^{2+}, a proton of the coordinated water molecule in the dimer is transferred so as to form an $N_{(1)}\ldots H^+\ldots O^-_\gamma$ hydrogen bond. The γ-phosphate group in the $(ZnATP^{2+})_2H^+OH^-$ complex remains hydrated upon this transfer of H^+. According to the above estimates, $K_{a, Cy}$ for the coordinated H_2O molecule in Cy($CuATP^{2-}$) is 8.24×10^{-9} mol/l at 25°C; for the $ZnATP^{2-} \cdot OH_2$ complex, $K_{a, Cy} = 0.84 \times 10^{-9}$ mol/l. The anticipated structure of the dimer is shown in the scheme (a). In the calculation of the mole fraction of the $(CuATP^{2-})_2$ dimer, we set the dimerization constant to be $K'_D = [D]_0/[Cy_0]^2 = 200$ l/mol. Calculations using mathematical modeling methods have verified the assumption that the Zn^{2+} and Cu^{2+} dimers have similar geometries and are characterized by similar K'_D values. It is likely that the difference between the formal hydrolysis kinetics of the dimeric complexes $(ZnATP^{2+})_2H^+OH^-$ and $(CuATP^{2-})_2$ (both of which consist of two Cy($MATP^{2-}$) dimers) arises from the difference in the way the proton is detached from the H_2O molecule coordinated to M^{2+}. This H_2O molecule belongs to an $MATP^{2-}$ molecule in conformation **B**, and its deprotonation yields a coordinated $M^{2+}OH^-$ ion, which is an active nucleophile.

Figure 7 plots $w_{0, ADP}/[D]_0$ versus $1/[H_3O^+]$ for series I runs. In the pH range 5.2–6.3, the plot is linear, indicating that D and OH^- are involved in the initial ADP accumulation rate equation for the ascending branch of the rate-vs.-pH curve (that is, the species active in ADP formation is DOH^-). The same plot for experimental series II is presented in Fig. 8. The anticipated structure of the DOH^- species is shown in Scheme 1b.

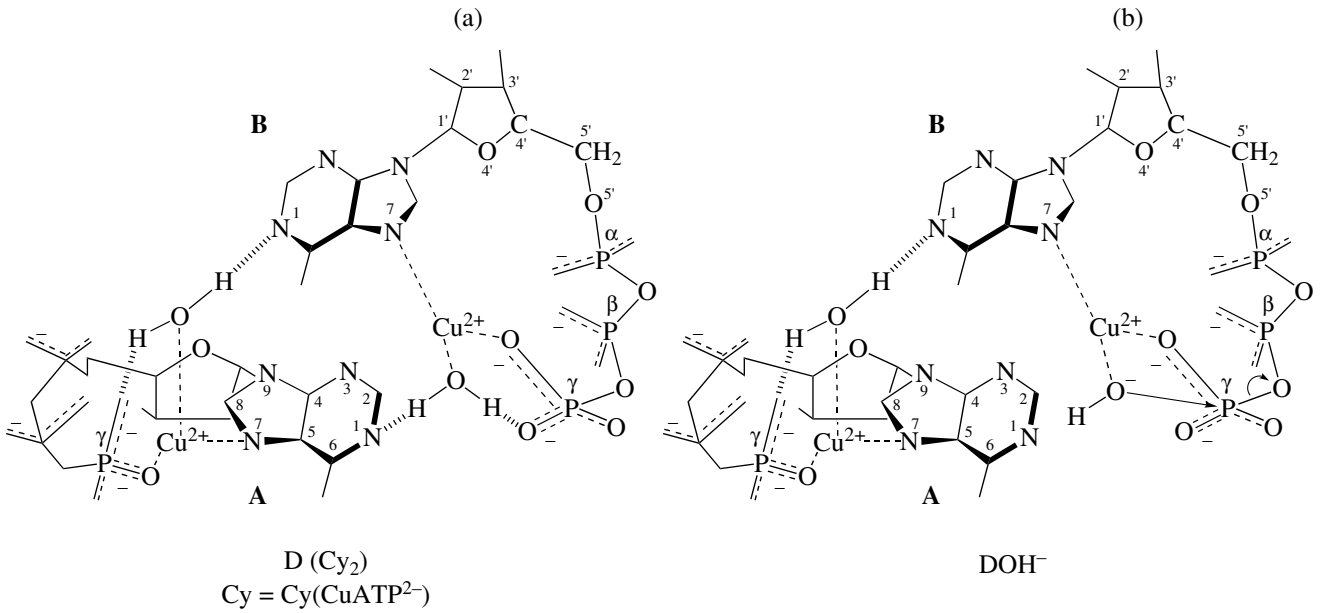

Scheme 1.

For pH ≥ pH$_{max}$, the $w_{0,\,ADP}/[D]_0$ ratio is pH-independent at the initial stage of hydrolysis (Figs. 7, 8). Therefore, the DOH$^-$ concentration that is the highest possible for a given pH is reached at the initial stage of hydrolysis, this concentration as a function of pH passes through a maximum, and ADP forms from DOH$^-$ at a rather high rate. The DOH$^-$ mole fraction maximum, which is reached in the initial portion of the ADP accumulation curve, occurs at a lower pH in series II than in series I.

The subsequent decrease in the ADP formation rate in the course of the process is more pronounced, the higher the pH is in the ascending branch of the rate-vs.-pH curve (see Fig. 3 and the results of runs 11–13 in Table 2). This decrease is apparently due to the formation of additional hydrolysis intermediates with the participation of OH$^-$ ions. One of these intermediates is responsible for the formation of AMP.

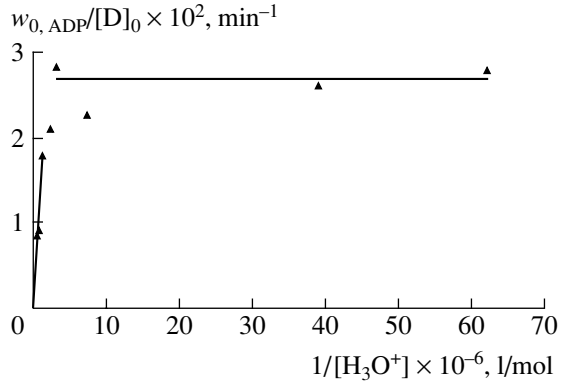

Fig. 8. Apparent ADP formation rate constant ($w_{0,\,ADP}/[D]_0$) versus $1/[H_3O^+]$ for the hydrolysis of the dimeric complex (CuATP$^{2-} \cdot OH_2)_2$ in series II runs at 25°C.

In all runs, after the $w_{0,\,ADP}$ maximum is reached, the ADP formation rate declines (at a given pH) and the attainment of a steady state by the hydrolysis process is pH-independent starting at an ATP conversion of ≈26% (Table 2). Therefore some equilibrium between DOH$^-$ and the intermediates responsible for DOH$^-$ deactivation is established on the descending branch of the $w_{0,\,ADP}$ curve. One of these intermediates is converted into AMP, and, as a consequence, the mole fraction of the resulting AMP is almost pH-independent at the final, steady-state stage of hydrolysis (Table 2).

REFERENCES

1. Sigel, H., Hofstetter, F., Martin, R.B., et al., *J. Am. Chem. Soc.*, 1984, vol. 106, no. 25, p. 7935.
2. Sigel, H., *Coord. Chem. Rev.*, 1990, vol. 100, p. 453.
3. Kochetkov, S.P., Gabibov, A.G., and Severin, E.S., *Bioorg. Khim.,* 1984, vol. 10, no. 10, p. 1301.
4. Mildvan, A.S., *Annu. Rev. Biochem.,* 1974, vol. 43, p. 357.
5. Sigel, H., in *Metal–DNA Chemistry*, Tullius, T.D., Ed., Washington, DC: Am. Chem. Soc., 1989.
6. De Meis, L., Behrens, M.I., Celis, H., et al., *Eur. J. Biochem.*, 1986, vol. 158, no. 1, p. 149.
7. De Meis, L., *FEBS Lett.*, 1987, vol. 213, no. 2, p. 333.
8. Wolcott, R.G. and Boyer, P.D., *Biochem. Biophys. Res. Commun.,* 1974, vol. 57, no. 3, p. 709.
9. Kandpal, R.P., Stempel, K.E., and Boyer, P.D., *Biochemistry*, 1987, vol. 26, no. 6, p. 1512.
10. Kayalar, C., Rosing, J., and Boyer, P.D., *J. Biol. Chem.*, 1977, vol. 252, no. 8, p. 2486.

11. Abrahams, J.P., Leslie, A.G.W., Lutter, R., et al., *Nature*, 1994, vol. 370, p. 621.
12. Sigel, H. and Tribolet, R., *J. Inorg. Biochem.*, 1990, vol. 40, no. 2, p. 163.
13. Haight, G.P., *Coord. Chem. Rev.*, 1987, vol. 79, no. 3, p. 293.
14. Wang, X., Nelson, D.J., Trindle, C., et al., *J. Inorg. Biochem.*, 1997, vol. 68, no. 1, p. 7.
15. Yohannes, P.G., Plute, K.E., Mertes, M.P., et al., *Inorg. Chem.*, 1987, vol. 26, no. 11, p. 1751.
16. Buisson, D.H. and Sigel, H., *Biochim. Biophys. Acta*, 1974, vol. 343, p. 45.
17. Sigel, H., Scheller, K.H., and Milburn, R.M., *Inorg. Chem.*, 1984, vol. 23, no. 13, p. 1933.
18. Scheller, K.H., Hofstetter, F., Mitchell, P.R., et al., *J. Am. Chem. Soc.*, 1981, vol. 103, no. 2, p. 247.
19. Sigel, H., *Eur. J. Biochem.*, 1987, vol. 165, p. 65.
20. Sigel, H., Tribolet, R., Malini-Balakrishnan, R., et al., *Inorg. Chem.*, 1987, vol. 26, no. 13, p. 2149.
21. Tribolet, R., Martin, R.B., and Sigel, H., *Inorg. Chem.*, 1987, vol. 26, no. 5, p. 638.
22. Sigel, H., *Chem. Soc. Rev.*, 1993, vol. 22, p. 255.
23. Scheller, K.H. and Sigel, H., *J. Am. Chem. Soc.,* 1983, vol. 105, no. 18, p. 5891.
24. Ramirez, F. and Marecek, J.F., *Biochim. Biophys. Acta*, 1980, vol. 589, no. 1, p. 21.
25. Hediger, M. and Milburn, R.M., *J. Inorg. Biochem.*, 1982, vol. 16, no. 2, p. 165.
26. Tafesse, F., Massoud, S.S., and Milburn, R.M., *Inorg. Chem.,* 1985, vol. 17, p. 2591.
27. Massoud, S.S. and Milburn, R.M., *J. Inorg. Biochem.*, 1990, vol. 39, no. 4, p. 337.
28. Tafesse, F., Massoud, S.S., and Milburn, R.M., *Inorg. Chem.*, 1993, vol. 32, no. 9, p. 1864.
29. Massoud, S.S. and Milburn, R.M., *Inorg. Chim. Acta*, 1989, vol. 163, no. 1, p. 87.
30. Massoud, S.S. and Milburn, R.M., *Inorg. Chim. Acta*, 1988, vol. 148, no. 1, p. 233.
31. Massoud, S.S., *J. Inorg. Biochem.*, 1994, vol. 55, no. 3, p. 183.
32. Utyanskaya, E.Z., Lidskii, B.V., Neigauz, M.G., et al., *Kinet. Katal.*, 2000, vol. 41, no. 4, p. 511 [*Kinet. Catal.* (Engl. Transl.), vol. 41, no. 4, p. 462].
33. Utyanskaya, E.Z., Lidskii, B.V., Neihaus, M.G., et al., *J. Inorg. Biochem.,* 2000, vol. 81, no. 1, p. 239.
34. Utyanskaya, E.Z., Pavlovskii, A.G., Sosfenov, N.I., et al., *Kinet. Katal.*, 1989, vol. 30, no. 6, p. 1343.
35. Utyanskaya, E.Z., Pavlov, A.O., Orekhova, E.M., et al., *Kinet. Katal.*, 1991, vol. 32, no. 2, p. 349.
36. Utyanskaya, E.Z., Mikhailova, T.V., Pavlov, A.O., et al., *ACH—Models Chem.*, 1996, vol. 133, nos. 1–2, p. 65.
37. Utyanskaya, E.Z., Shilov, A.E., Lidskii, B.V., et al., *ACH—Models Chem.*, 1996, vol. 133, no. 4, p. 365.
38. Utyanskaya, E.Z., Lidskii, B.V., Neigauz, M.G., et al., *Kinet. Katal.*, 2002, vol. 43, no. 3, p. 346 [*Kinet. Catal.* (Engl. Transl.), vol. 43, no. 3, p. 316].
39. Utyanskaya, E.Z., Pavlov, A.O., Orekhova, E.M., et al., *Zh. Anal. Khim.*, 1990, vol. 45, no. 6, p. 1222.
40. Bhat, T.R. and Krishnamurthy, M., *J. Inorg. Nucl. Chem.*, 1963, vol. 25, p. 1147.